J. Cent. South Univ. (2014) 21: 3722−3735
DOI: 10.1007/s11771-014-2356-y

Springer

Dynamic probabilistic analysis of stress and deformation for bladed disk assemblies of aeroengine

BAI Bin(白斌), BAI Guang-chen(白广忱)

School of Energy and Power Engineering, Beijing University of Aeronautics and Astronautics, Beijing 100191, China

Abstract: In order to describe and control the stress distribution and total deformation of bladed disk assemblies used in the aeroengine, a highly efficient and precise method of probabilistic analysis which is called extremum response surface method (ERSM) is produced based on the previous deterministic analysis results with the finite element model (FEM). In this work, many key nonlinear factors, such as the dynamic feature of the temperature load, the centrifugal force and the boundary conditions, are taken into consideration for the model. The changing patterns with time of bladed disk assemblies about stress distribution and total deformation are obtained during the deterministic analysis, and at the same time, the largest deformation and stress nodes of bladed disk assemblies are found and taken as input target of probabilistic analysis in a scientific and reasonable way. Not only their reliability, historical sample, extreme response surface (ERS) and the cumulative probability distribution function but also their sensitivity and effect probability are obtained. Main factors affecting stress distribution and total deformation of bladed disk assemblies are investigated through the sensitivity analysis of the model. Finally, compared with the response surface method (RSM) and the Monte Carlo simulation (MCS), the results show that this new approach is effective.

Key words: bladed disk assemblies; probabilistic analysis; finite element model; extremum response surface method; sensitivity analysis; transient dynamic analysis

1 Introduction

As the heart of the aircraft, an aeroengine is a complex rotary mechanical equipment and usually works in poor environment involving high temperature, high pressure, high revolving speed and various heavy loads, including not only the classical ones such as the mechanical load and the centrifugal load, but also the gas temperature, which acts as the primary cause for failures or even accidents. Among all the failures of aeroengine, the number of failures on the bladed disk assemblies accounts for about 25%, which has a serious impact on the safety, reliability, robustness, efficiency and other performance of the aeroengine. For instance, the method presented by KENYON et al [1−4] considered two interval leaves which contain cracks and revealed their influence patterns on the structure vibration characteristics. Thereafter, KENYON et al [1] rebuilt his model in 2003 by attaching a continuous shear spring to the ring in which the stiffness was allowed to vary along the ring annulus. In the model, the sensitivity to harmonic small mistuning forced response of turbine engine bladed disks was also evaluated using the method of harmonic perturbations and the finite element model was optimized using the sensitivity coefficient method. The forced response of the mistuned sector within the bladed disk assemblies was investigated by PETROV [5], considering the influence of the aerodynamic force and frequency veering. The random forced dynamic response of mistuned bladed disk assemblies was studied through experimental methods by JUDGE et al [6] in which the piezoelectric actuator was introduced. The reduced order model (ROM) based on component modes synthesis (CMS) was presented by BLADH et al [7−8] and the probability of forced response of mistuned bladed disk assemblies was calculated. Compared with the Monte Carlo simulation (MCS), the computational efficiency of ROM was greatly improved, and then the novel secondary modal analysis reduction technique (SMART) was proposed to further improve the computational efficiency, but the precision was descended because of the two times of the reduced orders in the model. The high cycle fatigue and sensitivity correlated with the vibration response and fatigue life were studied by CHAN and EWINS [9]. Meanwhile, the maximum vibration response of the component structures was predicted. An approach accounting for the geometric differences with high fidelity and at a reasonable one-time cost was presented by HSU and HOYNIAK [10].

Foundation item: Projects(51375032, 51175017, 51245027) supported by the National Natural Science Foundation of China
Received date: 2013−05−29; **Accepted date:** 2013−10−05
Corresponding author: BAI Bin, PhD; Tel: +86−18810600993; E-mail: baibin@126.com

The approach was based on the influence-coefficient (IC) method together with a set of sensitivity coefficients which were defined for the blade geometry changing effects and made use of a set of principal component analysis (PCA) modes that described the measured blade geometry variation.

Among all of the above contributions, although bladed disk assemblies were studied in different aspects, only the deterministic analysis of the mechanical force was given, such as the harmonic cycle vibration force and aerodynamic force, while the randomness and uncertainty of structure deformation were widely ignored. However, the blisk structure of the aircraft engine is a rotor structure which works at high rotating speed and the influence of the centrifugal force and the coriolis forces can't be ignored because of the eddy current phenomenon. Furthermore, the high temperature can not be ignored either as it can cause the deformation of the bladed disk assemblies. However, few studies were conducted regarding this issue.

Although the effect of centrifugal force was considered by SOIZE et al [11], the probabilistic model was nonparametric. And NIKOLIC et al [12] only considered the influence of coriolis forces on the forced response of blisk, leaving all the other important factors unconsidered, such as mechanical force. In real working environment, the blisk of aeroengine is influenced by the combination of various complicated factors such as the mechanical force, the temperature, the coriolis forces, especially the speed (the centrifugal force), all of which are uncertain factors and change dynamically following the working status, so the randomness of those various factors should be considered and the probabilistic analysis should be conducted.

Based on the deficiency of the above contributions, the randomness and uncertainty of the input variables are considered in this work and the probabilistic analysis of the stress distribution and the total deformation of structure is studied. Probabilistic analysis has been widely used in the fields of water conservancy, civil construction, geology and so on [13−16]. Recently, it has been newly applied to the sensitivity of the mechanical structure analysis, the uncertainty analysis and the risk assessment and other fields [17−20]. Within all those applications, the one based on RSM is widely accepted and implemented. But the probabilistic analysis of the deformation of the bladed disk assemblies, which is complex, nonlinear and dynamic, can be converted into a random process. Therefore, the dynamic reliability analysis about the deformation of bladed disk assemblies using the traditional RSM method is not sufficient because of its long computation time and relatively low precision and efficiency, so the ERSM is proposed to conduct the dynamic probabilistic analysis (DPA) about it. This method can significantly improve the computational efficiency without reducing the precision, which makes it possible to set up the FEM of high-fidelity blisk structure. Meanwhile, the dynamic temperature load, the centrifugal force, the coriolis forces and the nonlinear feature of material properties are considered and random variables are reasonably selected. So the idea of combining the FEM and the ERSM which is called FE-ERSM is used for the DPA of bladed disk assemblies used in the aeroengine.

2 Basic principle of ERSM

2.1 Traditional probabilistic analysis method

The traditional probabilistic analysis method [21−26] mainly includes the finite difference method (FDM), first-order second-moment method (FOSM), neural network method (NNM), Monte Carlo simulate (MCS), response surface method (RSM) and so on.

The FDM is easy to implement, but structural failure probability needs to be computed repeatedly and is not sufficient because of its long computation time. Also, the step length is difficult to determine. What is worse, wrong step will lead to wrong conclusions. The FOSM is mainly used in the linear limit state equation (LSE) and it has great dependence on the explicit expression. The NNM can effectively solve abnormal distribution, nonlinear problems, etc, but the randomness is stronger. So if you want to get a good neural network structure and need to debug artificially, it costs lots of time and needs many persons, and this method has no fundamental statistical theory. The explanation is not strong, so the application is limited to a great extent. Although MCS can study the randomness of the problem and the convergence speed has nothing to do with dimension, it is very slow and needs to emulate enough cycles to get reasonable result. It not only requires a lot of time but also the efficiency is not every high. There is no "memory" function in the process of sample drawn, that is, if there are several parameters in the random input parametric space, but these data do not provide new information in the process of calculation which is equivalent to repeat operation, then the research is effective for bits of random variables and steady state analysis for simple system. Probabilistic analysis of the bladed disk assemblies needs to consider the dynamics of the load, material properties, nonlinearity of boundary conditions, etc., so the amount of calculation increases greatly and can't meet the requirements. The experimental points and the iteration strategy are selected reasonably by RSM through a series of deterministic experiments, so as to determine the unknown coefficients in the expression ultimately. The analytic expression is obtained. It ignores the complicated original relationship

in the system and the input and output relation of the system is simulated by the response surface function (RSF), so it is also called surrogate model.

The computational process is as follows:

1) Assume that the relation about the output response with the vector of random input parameters $\boldsymbol{X}=[X_1, X_2, \cdots, X_r]$ affecting the structure is described as a quadratic function containing cross terms, namely

$$\hat{Y}(X_i)=a+\sum_{i=1}^{r}b_iX_i+\sum_{i=1}^{r}\sum_{j=i}^{r}c_{ij}X_iX_j \tag{1}$$

where a, b_i and c_{ij} (i=1, ⋯, r; j=1, ⋯, r) are respectively constant item, linear and quadratic undetermined coefficients.

It can be also described as matrix

$$\hat{\boldsymbol{Y}}(X_i)=\boldsymbol{A}+\boldsymbol{B}\boldsymbol{X}+\boldsymbol{X}^{\mathrm{T}}\boldsymbol{C}\boldsymbol{X} \tag{2}$$

where $\boldsymbol{B}$, $\boldsymbol{C}$ and $\boldsymbol{X}^{(j)}$ are shown in Eqs. (3)−(5)

$$\boldsymbol{B}=[b_1\ b_2\ \cdots\ b_r] \tag{3}$$

$$\boldsymbol{C}=\begin{bmatrix} c_{11} & & & & \\ c_{21} & c_{22} & & & \\ c_{31} & c_{32} & c_{33} & & \\ \vdots & \vdots & \vdots & & \\ c_{r1} & c_{r2} & c_{r3} & \cdots & c_{rr} \end{bmatrix} \tag{4}$$

$$\boldsymbol{X}^{(j)}=[x_1^{(j)}\ x_2^{(j)}\ \cdots\ x_r^{(j)}]^{\mathrm{T}} \tag{5}$$

where $\boldsymbol{A}$, $\boldsymbol{B}$, $\boldsymbol{C}$ and $\boldsymbol{X}^{(j)}$ are respectively constant item, linear coefficient matrix, quadratic coefficient matrix, input variable and r is the number of input variables.

2) The number of sample points $s=\dfrac{(1+r)(2+r)}{2}$. s sample points of random parameter vector are obtained using someway sample drawn, then these sample points are put into the Eq. (1) or Eq. (2) and a equation set is formed which is composed of s equations and the undetermined coefficient can be solved.

3) These sample points are tested and a set of sample points $(\hat{Y}_1, \hat{Y}_2, \cdots, \hat{Y}_r)$ of output response are obtained.

4) Least squares estimate is obtained through regression analysis (RA), and then the RSF is obtained. In fact, the sample points are numerically simulated and the output response is got using the LSRA for these data. That is to say, difference of square about the RSF $\hat{Y}(X_i)$ with the curved surface $Y(X_i)$ of the real limit state function (LSF) is minimal, and its expression is

$$\Delta Y=\min\sum_{i=1}^{s}[Y(X_i)-\hat{Y}(X_i)]^2 \tag{6}$$

Namely

$$\Delta Y=\min\sum_{i=1}^{s}\left[Y(X_i)-a\sum_{i=1}^{r}b_iX_i-\sum_{i=1}^{r}\sum_{j=1}^{r}c_{ij}X_iX_j\right]^2 \tag{7}$$

And

$$\begin{cases} \dfrac{\partial\Delta Y}{\partial a}=0 \\ \dfrac{\partial\Delta Y}{\partial b_i}=0,\ i=1,2,\cdots,r \\ \dfrac{\partial\Delta Y}{\partial c_{ij}}=0,\ i=1,\cdots,r;\ j=1,\cdots,r \end{cases} \tag{8}$$

It is calculated and then the expression of the quadratic RSF is determined.

5) The real response of the structure is replaced by the RSF which can be used to replace the FEM for probabilistic analysis and then the limit state function equation (LSFE) is achieved.

Compared with MCS, computational efficiency of this method is improved, but probabilistic analysis of the deformation of bladed disk assemblies used in aeroengine is a complex nonlinear dynamic problem which is not sufficient because of its long computation time and relatively low precision and efficiency, so ERSM is proposed to do the DPA.

2.2 ERSM of DPA

2.2.1 Basic principle of ERSM

Firstly, random samples of input parameters are small-lot extracted through MCS and system dynamics equation is solved for each sample and dynamic output response of system in the time domain [0, T] is got. Secondly, the extrema of dynamic output responses corresponding to all input samples are regarded as new output responses which are called extreme output responses (EORs), and then the function between input parameters and EOR is constructed which is called ERSF in the time domain [0, T]. An s set of input variable and its corresponding output ERS are selected and put into ERSF and the RSF coefficients are got. Finally, system reliability is calculated by ERSF which is called ERSM, that is, a large number of sampling is extracted and taken into ERSF and then dynamic EOR of system is calculated, so the reliability of the system is obtained.

And the FEM for each sample is analysed in the time domain [0, T] in this work and then it is replaced by this ERSF to calculate dynamic output response (DOR) of system. This method does not calculate every moment of output response and only calculates different extreme values of output response corresponding to input random variables in the time domain [0, T], and then samples are extracted using MCS and put into ERSF which is used to

replace the FEM to calculate DOR of system for the probabilistic analysis called DPA of FE-ERSM. The process of probabilistic analysis is shown in Fig. 1. It is shown that complicated nonlinear DPA of the random process is transformed into random variables, which can fully consider the dynamic influence of random input parameters on output parameters. There is no need to calculate the output response of every moment, and only the output response extremum of different input random variables is needed. Thus, the computing time can be greatly reduced and the computational efficiency can be improved. At the same time, computational precision is ensured, and some impossible problems of probabilistic analysis can be realized.

2.2.2 Mathematical model of ERSM

As shown in Fig. 2, assume that the j set of input samples of FEM is $\boldsymbol{X}^{(j)}$, output response is $\boldsymbol{Y}^j(t, \boldsymbol{X}^j)$ in the time domain [0, T] whose maximum value is $\boldsymbol{Y}^j_{\max}(\boldsymbol{X}^j)$ and then make a set $\{\boldsymbol{Y}^{(j)}_{\max}(\boldsymbol{X}^{(j)} : j \in \boldsymbol{Z}_+)\}$ and curve fitted through numerical points as a new output response curve $\boldsymbol{Y}$:

$$\boldsymbol{Y} = f(\boldsymbol{X}) = \{\boldsymbol{Y}^{(j)}_{\max}(\boldsymbol{X}^{(j)}) : j \in \boldsymbol{Z}_+\} \tag{9}$$

Equation (9) is written as the ERSF which is shown in Eq. (10):

$$\boldsymbol{Y}_{\max} = \boldsymbol{A} + \boldsymbol{B}\boldsymbol{Y}^j_{\max} + (\boldsymbol{Y}^j_{\max})^{\mathrm{T}}\boldsymbol{C}\boldsymbol{Y}^j_{\max} \tag{10}$$

Order $\boldsymbol{X} = \boldsymbol{Y}^j_{\max}$, and Eq. (10) is changed into

$$\boldsymbol{Y}_{\max}(\boldsymbol{X}) = \boldsymbol{A} + \boldsymbol{B}\boldsymbol{X} + \boldsymbol{X}^{\mathrm{T}}\boldsymbol{C}\boldsymbol{X} \tag{11}$$

And $\boldsymbol{B}$, $\boldsymbol{C}$ and $\boldsymbol{X}^{(j)}$ are shown in Eqs. (12)−(14):

$$\boldsymbol{B}=[b_1 \ b_2 \ \cdots \ b_r] \tag{12}$$

$$\boldsymbol{C} = \begin{bmatrix} c_{11} & & & & \\ c_{21} & c_{22} & & & \\ c_{31} & c_{32} & c_{33} & & \\ \vdots & \vdots & \vdots & & \\ c_{r1} & c_{r2} & c_{r3} & \cdots & c_{rr} \end{bmatrix} \tag{13}$$

$$\boldsymbol{X}^{(j)} = [x_1^{(j)} \ x_2^{(j)} \ \cdots \ x_r^{(j)}]^{\mathrm{T}} \tag{14}$$

where r is the number of input variable.

Sufficient test points are selected and the test data are brought into Eq. (10) or Eq. (11). The coefficients $\boldsymbol{A}$, $\boldsymbol{B}$ and $\boldsymbol{C}$ of ERSF are determined and the expressions of them are obtained to replace probabilistic analysis of the FEM.

3 Probabilistic analysis method

3.1 Reliability calculation

Probabilistic design is an analysis technique for assessing the effect of uncertain input parameters and assumptions on a model to determine the distribution of results and over-design can be avoided and quantitative

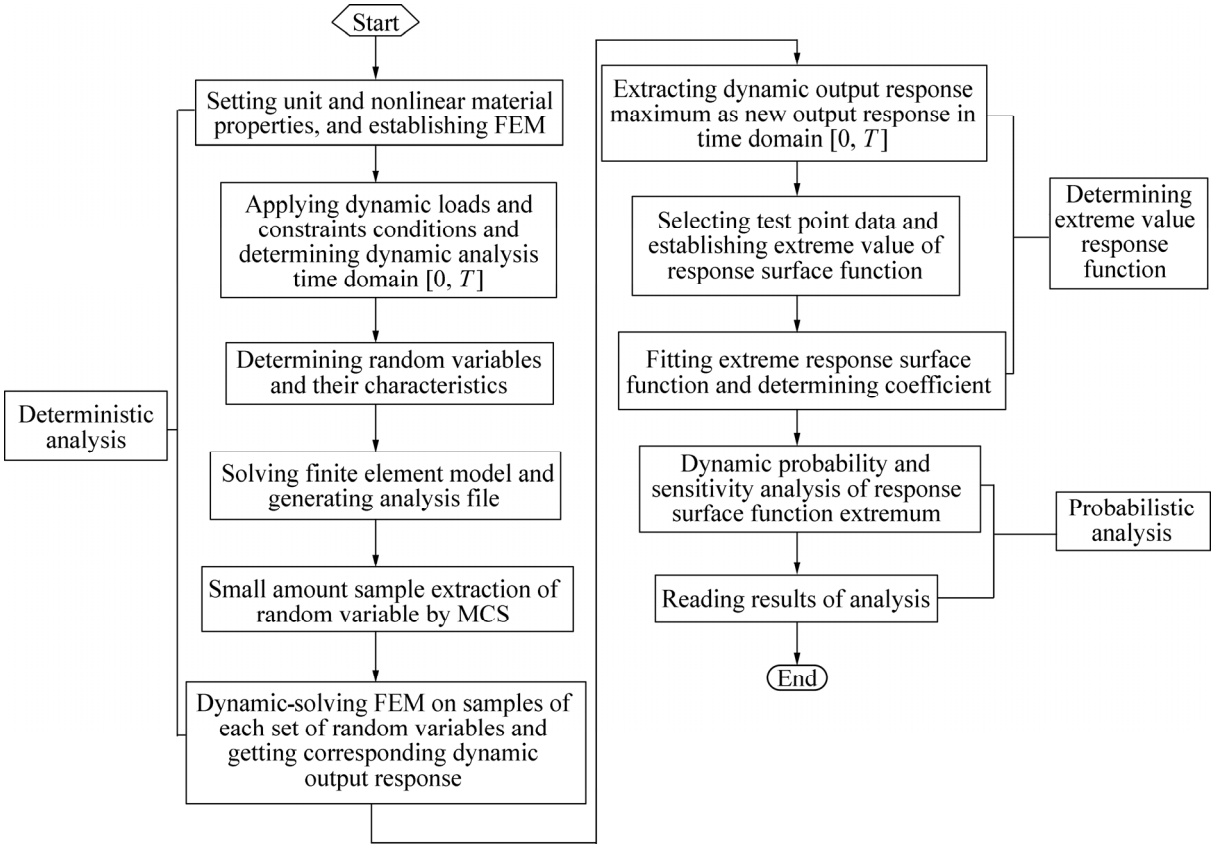

Fig. 1 Flow chart of DPA of FE-ERSM

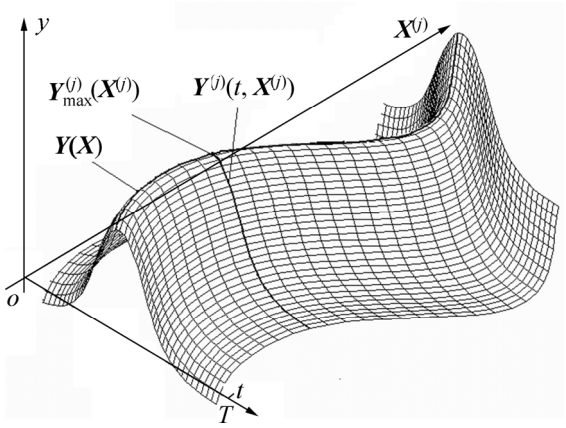

Fig. 2 Principle diagram of FE-ERSM

results for reliability of parts under operating conditions can be given to ensure its safety. If its real output is $\boldsymbol{Y}(\boldsymbol{X})$ after RSF determined, then its LSF is

$$\boldsymbol{g}(\boldsymbol{X})=\boldsymbol{Y}(\boldsymbol{X})-\hat{\boldsymbol{Y}}(\boldsymbol{X}) \tag{15}$$

i.e.,

$$\boldsymbol{g}(\boldsymbol{X})=\boldsymbol{Y}(\boldsymbol{X})-\boldsymbol{A}-\boldsymbol{B}\boldsymbol{X}-\boldsymbol{X}^{\mathrm{T}}\boldsymbol{C}\boldsymbol{X} \tag{16}$$

From Eq. (16), it not only contains linear and quadratic item but also includes quadratic cross item information in $\boldsymbol{g}(\boldsymbol{X})$, so that the reliability and sensitivity computational precision is guaranteed. If $\boldsymbol{g}(\boldsymbol{X})<0$, it is a failure mode, otherwise, it is a safe mode. And if each variable is independent of each other and their mean and variance matrix are $\boldsymbol{\mu}=[\mu_1, \mu_2, \cdots, \mu_r]$ and $\boldsymbol{D}=[\sigma_1, \sigma_2, \cdots, \sigma_r]$, i.e.

$$\begin{cases} E(c)=c \\ E(aX_i)aE(X_i)=a_i\mu_i \\ E(X_iX_j)=E(X_i)E(X_j)=\mu_i\mu_j \\ E(aX_i+bX_j)=aE(X_i)+bE(X_j)=a\mu_i+b\mu_j \\ E(X_i^2)=E^2(X_i)+D(X_i)=\mu_i^2+\sigma_i^2 \\ D(c)=0 \\ D(aX_i)=a^2D(X_i)+b^2D(X_j)=a^2\sigma_i^2+b^2\sigma_j^2 \\ D(X_i^2)=4\mu_i^2\sigma_i^2 \\ D(X_iX_j)=\mu_i^2\sigma_j^2+\mu_j^2\sigma_i^2+\sigma_i^2\sigma_j^2 \end{cases} \tag{17}$$

So mean and variance matrices of $\boldsymbol{g}(\boldsymbol{X})$ are

$$E[g(\boldsymbol{X})]=\mu_g(\mu_1,\mu_2,\cdots,\mu_r,\mu_\delta,\sigma_1^2,\sigma_2^2,\cdots,\sigma_r^2,\sigma_\delta^2) \tag{18}$$

$$D[g(\boldsymbol{X})]=D_g(\mu_1,\mu_2,\cdots,\mu_r,\mu_\delta,\sigma_1^2,\sigma_2^2,\cdots,\sigma_r^2,\sigma_\delta^2) \tag{19}$$

Because the random variables are independent of each other, the LSF obeys Gaussian distribution and the reliability index and degree of reliability are respectively

$$\beta=\frac{\mu_g}{\sqrt{D_g}} \tag{20}$$

$$R=\Phi(\beta) \tag{21}$$

where $\Phi(\cdot)$ is standard normal distribution.

3.2 Sensitivity analysis

Generally, reliability sensitivity is defined as the failure probability for partial derivatives to basic variables distribution parameters. The failure probability P_{F} is given as

$$P_{\mathrm{F}}=1-R \tag{22}$$

And the sensitivity of failure probability is

$$\begin{cases} \dfrac{\partial P_{\mathrm{F}}}{\partial \boldsymbol{\mu}}=\dfrac{1}{r}\displaystyle\sum_{i=1}^{r}\frac{\partial P_{fi}}{\partial \mu_{xi}}=\frac{\partial(1-R)}{\partial \boldsymbol{\mu}} \\ \dfrac{\partial P_{\mathrm{F}}}{\partial \sigma_x}=\dfrac{1}{r}\displaystyle\sum_{i=1}^{r}\frac{\partial P_{fi}}{\partial \sigma_{xi}}=\frac{\partial(1-R)}{\partial \sigma_x} \end{cases} \tag{23}$$

That is

$$\begin{cases} \dfrac{\partial R}{\partial \boldsymbol{\mu}}=\dfrac{\partial R}{\partial \beta}\left(\dfrac{\partial \beta}{\partial \mu_g}\dfrac{\partial \mu_g}{\partial \boldsymbol{\mu}}+\dfrac{\partial \beta}{\partial D_g}\dfrac{\partial D_g}{\partial \boldsymbol{\mu}}\right) \\ \dfrac{\partial R}{\partial D}=\dfrac{\partial R}{\partial \beta}\left(\dfrac{\partial \beta}{\partial \mu_g}\dfrac{\partial \mu_g}{\partial D}+\dfrac{\partial \beta}{\partial D_g}\dfrac{\partial D_g}{\partial D}\right) \end{cases} \tag{24}$$

And

$$\begin{cases} \dfrac{\partial R}{\partial \beta}=\varphi(\beta) \\ \dfrac{\partial R}{\partial \mu_{\mathrm{g}}}=\dfrac{1}{\sigma_g} \\ \dfrac{\partial \mu_g}{\partial \boldsymbol{\mu}}=\left(\dfrac{\partial \mu_g}{\partial \mu_1},\dfrac{\partial \mu_g}{\partial \mu_2},\cdots,\dfrac{\partial \mu_g}{\partial \mu_r}\right) \\ \dfrac{\partial \mu_g}{\partial D_g}=-\dfrac{\mu_g}{2}D_g^{-\frac{3}{2}} \\ \dfrac{\partial D_g}{\partial \boldsymbol{\mu}}=\left(\dfrac{\partial D_g}{\partial \mu_1},\dfrac{\partial D_g}{\partial \mu_2},\cdots,\dfrac{\partial D_g}{\partial \mu_r}\right) \\ \dfrac{\partial \mu_g}{\partial D}=\left(\dfrac{\partial \mu_g}{\partial \sigma_1^2},\dfrac{\partial \mu_g}{\partial \sigma_2^2},\cdots,\dfrac{\partial \mu_g}{\partial \sigma_r^2}\right) \\ \dfrac{\partial D_g}{\partial D}=\left(\dfrac{\partial D_g}{\partial \sigma_1^2},\dfrac{\partial D_g}{\partial \sigma_2^2},\cdots,\dfrac{\partial D_g}{\partial \sigma_r^2}\right) \end{cases} \tag{25}$$

The reliability sensitivity shown in Eq. (23) or Eq. (24) is approximate and there is a lot of randomness if the sample size is small. But on the basis of law of large numbers, estimates of Eq. (23) or Eq. (24) with the increase of sample size gradually tend to be the true values. Mean and variance of reliability sensitivity need to be analysed in order to better understand convergence

and precision. The overall mean and variance can be replaced by sample mean and variance also because of independence among samples, i.e.

$$\begin{cases} E\left(\dfrac{\partial P_{\mathrm{F}}}{\partial \boldsymbol{\mu}}\right)=E\left(\dfrac{1}{r}\sum\limits_{i=1}^{r}\dfrac{\partial P_{fi}}{\partial \mu_{xi}}\right)=E\left(\dfrac{\partial(1-R)}{\partial \boldsymbol{\mu}}\right) \\ \mathrm{Var}\left(\dfrac{\partial P_{\mathrm{F}}}{\partial \boldsymbol{\mu}}\right)=\mathrm{Var}\left(\dfrac{1}{r}\sum\limits_{i=1}^{r}\dfrac{\partial P_{fi}}{\partial \mu_{xi}}\right)=\mathrm{Var}\left(\dfrac{\partial(1-R)}{\partial \boldsymbol{\mu}}\right) \\ E\left(\dfrac{\partial P_{\mathrm{F}}}{\partial \sigma_X}\right)=E\left(\dfrac{1}{r}\sum\limits_{i=1}^{r}\dfrac{\partial P_{fi}}{\partial \sigma_{xi}}\right)=E\left(\dfrac{\partial(1-R)}{\partial \sigma_X}\right) \\ \mathrm{Var}\left(\dfrac{\partial P_{\mathrm{F}}}{\partial \sigma_X}\right)=\mathrm{Var}\left(\dfrac{1}{r}\sum\limits_{i=1}^{r}\dfrac{\partial P_{fi}}{\partial \sigma_{xi}}\right)=\mathrm{Var}\left(\dfrac{\partial(1-R)}{\partial \sigma_X}\right) \end{cases} \tag{26}$$

i.e.

$$\begin{cases} E\left(\dfrac{\partial R}{\partial \boldsymbol{\mu}}\right)=E\left[\dfrac{\partial R}{\partial \beta}\left(\dfrac{\partial \beta}{\partial \mu_g}\dfrac{\partial \mu_g}{\partial \boldsymbol{\mu}}+\dfrac{\partial \beta}{\partial D_g}\dfrac{\partial D_g}{\partial \boldsymbol{\mu}}\right)\right] \\ \quad =\varphi(\beta)\dfrac{1}{\sigma_g}E\left(\dfrac{\partial \mu_g}{\partial \boldsymbol{\mu}}\right)+\varphi(\beta)\left(-\dfrac{\mu_g}{2}D_g^{-\frac{3}{2}}\right)\cdot \\ \quad E\left(\dfrac{\partial D_g}{\partial \boldsymbol{\mu}}\right) \\ \mathrm{Var}\left(\dfrac{\partial R}{\partial \boldsymbol{\mu}}\right)=\mathrm{Var}\left[\dfrac{\partial R}{\partial \beta}\left(\dfrac{\partial \beta}{\partial \mu_g}\dfrac{\partial \mu_g}{\partial \boldsymbol{\mu}}+\dfrac{\partial \beta}{\partial D_g}\dfrac{\partial D_g}{\partial \boldsymbol{\mu}}\right)\right] \\ \quad =\varphi^2(\beta)\sigma_g^{-2}\mathrm{Var}\left(\dfrac{\partial \mu_g}{\partial \boldsymbol{\mu}}\right)+\varphi^2(\beta)\left(-\dfrac{1}{4}\mu_g^2D_g^{-3}\right)\cdot \\ \quad \mathrm{Var}\left(\dfrac{\partial D_g}{\partial \boldsymbol{\mu}}\right) \\ E\left(\dfrac{\partial R}{\partial D}\right)=E\left[\dfrac{\partial R}{\partial \beta}\left(\dfrac{\partial \beta}{\partial \mu_g}\dfrac{\partial \mu_g}{\partial D}+\dfrac{\partial \beta}{\partial D_g}\dfrac{\partial D_g}{\partial D}\right)\right] \\ \quad =\varphi(\beta)\dfrac{1}{\sigma_g}E\left(\dfrac{\partial \mu_g}{\partial D}\right)+\varphi(\beta)\left(-\dfrac{\mu_g}{2}D_g^{-\frac{3}{2}}\right)\cdot \\ \quad E\left(\dfrac{\partial D_g}{\partial D}\right) \\ \mathrm{Var}\left(\dfrac{\partial R}{\partial D}\right)=\mathrm{Var}\left[\dfrac{\partial R}{\partial \beta}\left(\dfrac{\partial \beta}{\partial \mu_g}\dfrac{\partial \mu_g}{\partial D}+\dfrac{\partial \beta}{\partial D_g}\dfrac{\partial D_g}{\partial D}\right)\right] \\ \quad =\varphi^2(\beta)\sigma_g^{-2}\mathrm{Var}\left(\dfrac{\partial \mu_g}{\partial D}\right)+\varphi^2(\beta)\left(-\dfrac{1}{4}\mu_g^2D_g^{-3}\right)\cdot \\ \quad \mathrm{Var}\left(\dfrac{\partial D_g}{\partial D}\right) \end{cases} \tag{27}$$

The reliability sensitivity of the failure probability to the standard deviation of the variables in Eq. (23) or Eq. (24) is approximate and unbiased. So its variation coefficient in Eq. (28) or Eq. (29) is defined in order to reflect its relative dispersion, that is, the ratio of absolute value of the standard deviation to mathematical expectation:

$$\begin{cases} \mathrm{Cov}\left(\dfrac{\partial P_F}{\partial \boldsymbol{\mu}}\right)=\dfrac{\sqrt{\mathrm{Var}\left(\dfrac{\partial P_F}{\partial \boldsymbol{\mu}}\right)}}{\left|E\left(\dfrac{\partial P_F}{\boldsymbol{\mu}}\right)\right|}=\mathrm{Cov}\left(\dfrac{\partial(1-R)}{\partial \boldsymbol{\mu}}\right)=\dfrac{\sqrt{\mathrm{Var}\left(\dfrac{\partial(1-R)}{\partial \boldsymbol{\mu}}\right)}}{\left|E\left(\dfrac{\partial(1-R)}{\partial \boldsymbol{\mu}}\right)\right|} \\ \mathrm{Cov}\left(\dfrac{\partial P_F}{\partial \sigma_X}\right)=\dfrac{\sqrt{\mathrm{Var}\left(\dfrac{\partial P_F}{\partial \sigma_X}\right)}}{\left|E\left(\dfrac{\partial P_F}{\partial \sigma_X}\right)\right|}=\mathrm{Cov}\left(\dfrac{\partial(1-R)}{\partial \sigma_X}\right)=\dfrac{\sqrt{\mathrm{Var}\left(\dfrac{\partial(1-R)}{\partial \sigma_X}\right)}}{\left|E\left(\dfrac{\partial(1-R)}{\partial \sigma_X}\right)\right|} \end{cases} \tag{28}$$

i.e.

$$\begin{cases} \mathrm{Cov}\left(\dfrac{\partial P_F}{\partial \boldsymbol{\mu}}\right)=\dfrac{\sqrt{\mathrm{Var}\left(\dfrac{\partial R}{\partial \boldsymbol{\mu}}\right)}}{\left|E\left(\dfrac{\partial R}{\boldsymbol{\mu}}\right)\right|}=\left[\varphi^2(\beta)\sigma_g^{-2}\mathrm{Var}\left(\dfrac{\partial \mu_g}{\partial \boldsymbol{\mu}}\right)\cdot\right. \\ \quad \left.\varphi^2(\beta)\left(-\dfrac{1}{4}\mu_g^2D_g^{-3}\right)\mathrm{Var}\left(\dfrac{\partial D_g}{\partial \boldsymbol{\mu}}\right)\right]^{1/2}\Big/\left|\varphi(\beta)\dfrac{1}{\sigma_g}\right. \\ \quad \left.E\left(\dfrac{\partial \mu_g}{\partial \boldsymbol{\mu}}\right)+\varphi(\beta)\left(-\dfrac{\mu_g}{2}D_g^{-\frac{3}{2}}\right)E\left(\dfrac{\partial D_g}{\partial \boldsymbol{\mu}}\right)\right| \\ \mathrm{Cov}\left(\dfrac{\partial P_F}{\partial D}\right)=\dfrac{\sqrt{\mathrm{Var}\left(\dfrac{\partial R}{\partial D}\right)}}{\left|E\left(\dfrac{\partial R}{D}\right)\right|}=\left[\varphi^2(\beta)\sigma_g^{-2}\mathrm{Var}\left(\dfrac{\partial \mu_g}{\partial D}\right)\varphi^2(\beta)\cdot\right. \\ \quad \left.\left(-\dfrac{1}{4}\mu_g^2D_g^{-3}\right)\mathrm{Var}\left(\dfrac{\partial D_g}{\partial D}\right)\right]^{1/2}\Big/\left|\varphi(\beta)\dfrac{1}{\sigma_g}E\left(\dfrac{\partial \mu_g}{\partial D}\right)+\right. \\ \quad \left.\varphi(\beta)\left(-\dfrac{\mu_g}{2}D_g^{-\frac{3}{2}}\right)E\left(\dfrac{\partial D_g}{\partial D}\right)\right| \end{cases} \tag{29}$$

4 Heat transfer analysis of bladed disk assemblies

Deformation of turbine bladed disk assemblies used in the aeroengine is impacted in addition to the centrifugal load, the mechanical load and the aerodynamic load. Moreover, gas temperature also can't be ignored involving the heat transfer, the heat exchange and thermal boundary conditions, etc [27−28].

4.1 Differential equation of heat conduction

In cylindrical coordinates, according to the Fourier's law, three-dimensional transient heat conduction differential equation is established in the temperature field as

$$\rho c\frac{\partial T}{\partial \tau}=\frac{1}{r}\frac{\partial}{\partial r}\left(k_r r\frac{\partial T}{\partial r}\right)+\frac{1}{r^2}\frac{\partial}{\partial \varphi}\left(k_\varphi\frac{\partial T}{\partial \varphi}\right)+\frac{\partial T}{\partial z}\left(k_z\frac{\partial T}{\partial z}\right) \tag{30}$$

where r, φ and z are coordinates in the temperature field of bladed disk assemblies, ρ is density of materials, c is specific heat capacity and k_r, k_φ and k_z are heat conductivity coefficients.

4.2 Heat conduction

There is temperature difference that is the temperature gradient existing in the bladed disk assemblies. Heat can transfer from high temperature to low temperature in the blisk and it can transfer from high-temperature components to low- temperature components, so it satisfies equation of heat conduction as

$$\frac{Q}{t}=\frac{KA(T_{\text{hot}}-T_{\text{cold}})}{d} \tag{31}$$

where Q is heat flow rate within time t, K is heat conduction coefficient, T_{hot} is temperature of hyperthermal parts, T_{cold} is temperature of microthermal parts, d is thickness of bladed disk assemblies, and A is lateral area of bladed disk assemblies.

4.3 Thermal convection

The heat exchange occurs between the surface of aeroengine and the air flow contacting with it because of temperature difference, so there is thermal convection on the surface of the blisk according to the Newton cooling equation:

$$q''=\alpha|T_{\text{S}}-T_{\text{B}}| \tag{32}$$

And

$$\begin{cases}\alpha=\dfrac{Nu\lambda_{\text{c}}}{r}\\ Nu=0.45\beta Re^{0.80}\\ \beta=0.1313(1+\varepsilon^2)^{0.30}\left(0.08547\dfrac{v_{\text{a}}}{v_0}+0.3131\varepsilon\right)^{0.20}\\ Re=\dfrac{v_0 r}{v}=\dfrac{\omega r^2}{v}\\ \varepsilon=\sqrt{0.0262+0.4399\left(\dfrac{v_{\text{a}}}{v_0}\right)^2}-0.009362\dfrac{v_{\text{a}}}{v_0}\end{cases} \tag{33}$$

where α is convection coefficient, T_{s} is the surface temperature, T_{B} is air temperature, Re is Reynolds number, ω is rotational speed, r is the mean radius in the calculating area, v is dynamic viscosity coefficient of cooling air, v_{a} is axial velocity, and v_0 is peripheral speed.

4.4 Thermal boundary conditions

The heating boundary conditions and initial conditions must be given in order to make the heat balance equation of each node have unique solution, so the boundary conditions are the basis of thermal analysis. The temperature field calculation of aeroengine belongs to the heat conduction problem in heat transfer theory. There are three classes about the calculation of boundary conditions.

1) The temperature of the object boundary, i.e., the surface temperature distribution of bladed disk assemblies is given as

$$T|_{\Gamma}=f(x,\ y,\ z) \tag{34}$$

where Γ is the object boundary, and $f(\cdot)$ is the temperature function.

2) Heat flux of the object boundary, i.e., heat flow density of boundary surface of bladed disk assemblies is known as

$$-k\frac{\partial T}{\partial n}|_{\Gamma}=g(x,y,z,t) \tag{35}$$

where $g(\cdot)$ is heat flow density function, $\dfrac{\partial T}{\partial n}$ is temperature gradient of contact surface, and k is thermal conductivity coefficient of blisk.

3) The heat transfer coefficient and the environment temperature are given, which are called convective heat transfer boundary conditions. The process between the border and the external medium is given as

$$-k\frac{\partial T}{\partial n}|_{\Gamma}=h(T_{\text{w}}-T_{\text{f}}) \tag{36}$$

where h is heat transfer coefficient between the boundary and the surrounding air of blisk, T_{f} is surrounding air temperature, and T_{w} is surface temperature of structure boundary.

4.5 Initial condition

The initial condition is given as

$$T|_{\tau=0}\ (r,\ \varphi,\ z)=T_0\ (r,\ \varphi,\ z) \tag{37}$$

where T_0 is the initial temperature of blisk.

In some parts of blisk, temperature usually can be found in the technical file or got using the test method, such as at the outer fringe, center, wheel hub, so it can be regarded as the first kind of boundary condition. Normally, the heat transferring from disk to spindle is little, which can be neglected. Therefore, the joint of disk and spindle can be considered as adiabatic boundary. It can be regarded as special case of the second boundary condition which regards heat and heat flux density as zero. If flow pressure, temperature, quantity of flow, etc are given, exothermic coefficient can be calculated according to heat transfer formula, and lateral area of

disk and blade can be regarded as the third kind of boundary condition.

5 Deterministic analysis of bladed disk assemblies

5.1 Load spectrum calculation

The process including start−idling−take off−climbing−cruise of aeroengine taking off is selected in range of this study and 12 points [29−30] are taken as computing points, which more accord with the fact. And the influence of dynamic temperature, nonlinearity of material, heat conductivity coefficient, nonlinear expansion coefficient, specific heat, centrifugal force, coriolis forces, etc, are considered, so the dynamic thermal and structural coupling are researched and the load spectrum is shown in Fig. 3.

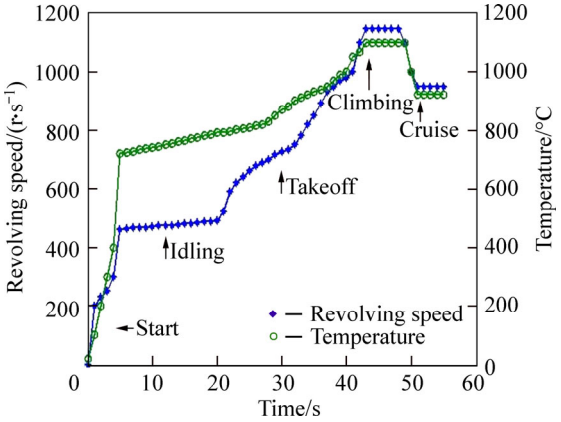

Fig. 3 Load spectrum of input variable

5.2 FEM of bladed disk assemblies

A certain type of II level high-pressure turbine blisk is selected as the research object, the cooling hole of blades, fillet of disk, etc, are simplified and a kind of material is called nickel alloy. The FEMs of bladed disk assemblies are shown in Fig. 4. Blisk is hypothetical as periodic structural system, meanwhile, machining error is not considered, so a sector is chosen as the research object, as shown in Fig. 5.

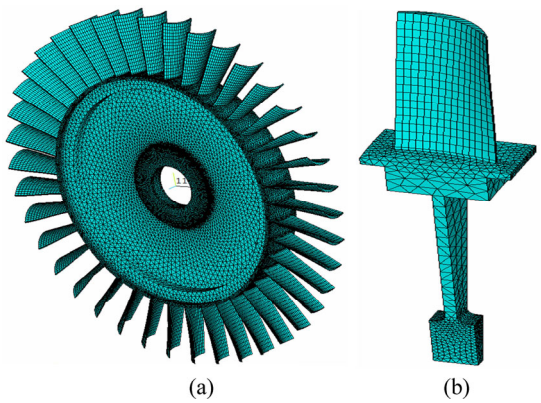

Fig. 4 FEMs of integral bladed disk assemblies (a) and single sector of bladed disk assemblies

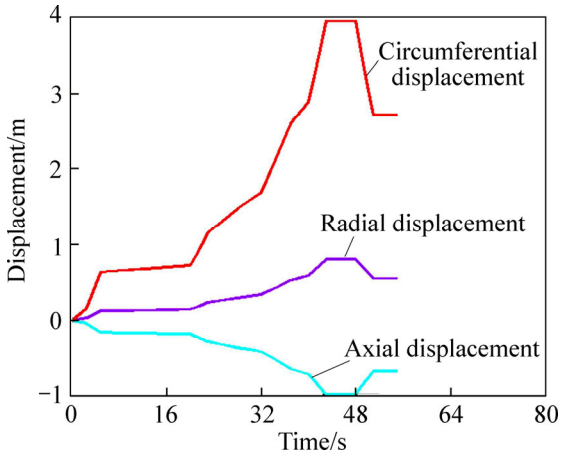

Fig. 5 Changing curve with time of bladed disk deformation

5.3 Deterministic analysis of bladed disk assemblies

According to the load spectrum of Fig. 3, transient dynamic analysis of sector of bladed disk assemblies shown in Fig. 5 is investigated and changing curve with time in Fig. 6 is got considering the effect of centrifugal and temperature load, and Coriolis forces, etc.

The research results show that rotational speed and gas temperature reach the maxima. Meanwhile, total deformation and stress also reach the maxima and the tangential deformation is larger than the radial and axial deformation. The stress is mainly concentrated at the blade root, and the total deformation occurs at the tip of blade when the plane climbs in the process. Actually, the phenomenon is mainly due to combining the centrifugal force, temperature and coriolis forces, which is consistent with the actual situation. Taking the most dangerous nodes as the research object, the stress distribution and total deformation are shown in Fig. 6.

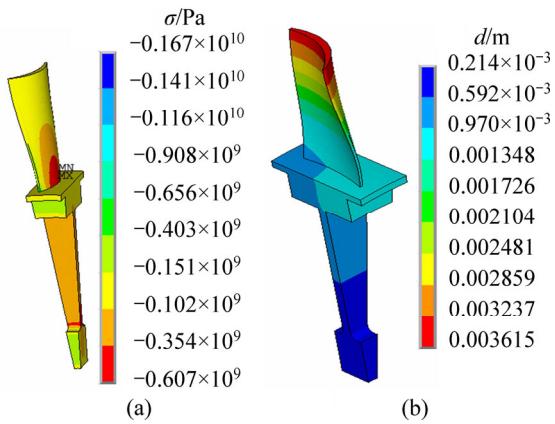

Fig. 6 Stress distribution (a) and total deformation (b) of bladed disk assemblies

6 DPA of bladed disk assemblies

6.1 Selection of random variable

There are some uncertain factors about the material

parameters and real working environment of bladed disk assemblies about aeroengine, so the selection of a random variable is more complex in the dynamic probability analysis than the steady state probabilistic analysis. As far as the impact of the input variables on the output responses is concerned, the traditional approach is that the influence of each input variable elements x_i (i=1, 2, ⋯, k) on the output responses is analyzed, then the comprehensive analysis and judgment are carried on. Each variable elements of this method needs to be considered and calculated, including cumbersome process, low efficiency and the comprehensive analysis of each element having no unified and effective rules, so the accuracy and the precision can not be guaranteed.

The probabilistic analysis is FEM parametric analysis, thus the selection of input variables is very important. The maximum selection method is used and the process is as follows:

1) The maximum of elements of a certain variable $\boldsymbol{X}_i$ in the input variables $\boldsymbol{X}$ is selected, namely, $x_{i,\max}$, then all elements divide it as

$$\boldsymbol{\alpha}=(\alpha_1, \alpha_2, \cdots, \alpha_k)=(x_1, x_2, \cdots, x_k)/x_{i,\max} \tag{38}$$

That is,

$$\boldsymbol{X}_i=(x_1, x_2, \cdots, x_k)=\boldsymbol{\alpha}\cdot x_{i,\max}=(\alpha_1, \alpha_2, \cdots, \alpha_k)\cdot x_{i,\max} \tag{39}$$

2) Array set $\widetilde{\boldsymbol{X}}=\{x_{1,\max}, x_{2,\max}, \cdots, x_{r,\max}\}$ is formed which is composed of the maximum of elements with every variable in $\boldsymbol{X}$=(X_1, X_2, ⋯, X_r). There is still a corresponding relationship between $\boldsymbol{X}$ and $\boldsymbol{Y}$ as shown in Eq. (40), if $\widetilde{\boldsymbol{X}}$ is written $\boldsymbol{Y}$, that is, $\boldsymbol{Y}$=(y_1, y_2, ⋯, y_r):

$$\boldsymbol{X}=(X_1, X_2, \cdots, X_r)\leftrightarrow\boldsymbol{Y}=(y_1, y_2, \cdots, y_r) \tag{40}$$

3) The effect of every element in the variable $\boldsymbol{X}_i$ on the output responses is analysed through researching the influence of $x_{i,\max}$ according to the correlation of them.

This method only needs to consider the effect of the maximum of a class variable on output responses and the number of random input variables is greatly reduced, which can obviously save computational time, improve the computational efficiency and precision, and provide conveniently for the DPA.

Random input variables of bladed disk assemblies are selected according to this method, involving rotational speed w, gas temperature t_r, expansion coefficient α, heat conductivity coefficient k, heat transfer coefficient f, specific heat capacity c, density ρ, elasticity modulus e and Poisson ratio v. Assume that all variables obey Gaussian distribution and they are independent of each other as shown in Table 1. Parts of the input variables of probability density and distribution function are shown in Figs. 7−10.

Table 1 Random input variables and numerical characteristics for bladed disk assemblies

Random variable	Mean, μ	Standard deviation, δ
w/(rad·s^{-1})	1046	20.92
t_r/°C	1200	24
α/10^{-5} °C	1.441	0.02882
k/(w·m^{-1}·°C^{-1})	27.21	0.5442
f/(w·m^{-1}·°C^{-1})	6320	126.4
c/(J·kg^{-1}·°C^{-1})	500	10
e/10^{11} Pa	1.48	0.0296
v	0.3143	0.00627
ρ/(kg·m^{-3})	8560	171.2

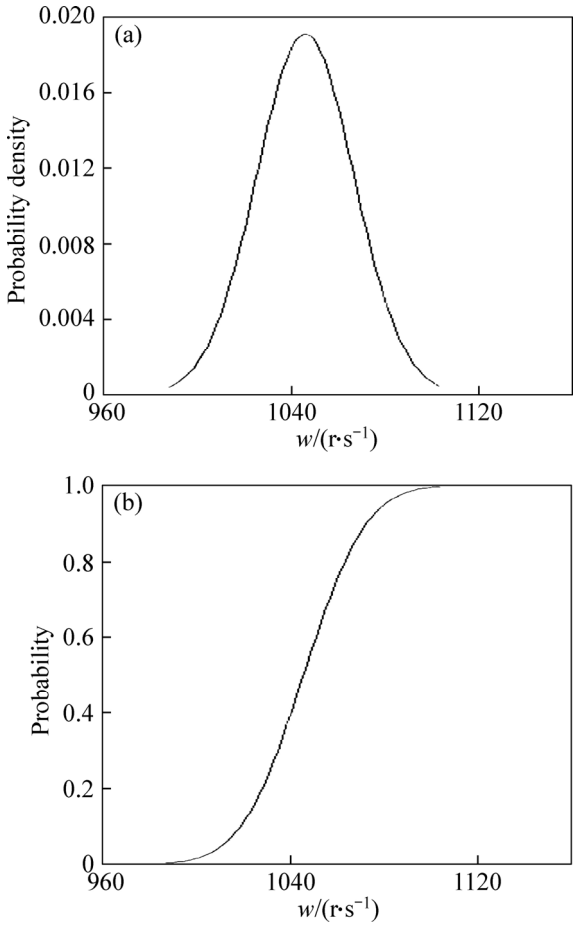

Fig. 7 Probability density (a) and distribution function (b) of rotational speed

6.2 Dynamic probabilistic analysis

LSE of stress distribution and total deformation for bladed disk assemblies are established in Eqs. (41)−(42), at the same time, the relationship of the ERS between the stress distribution or total deformation and any two input variables are obtained, as shown in Fig. 11.

$$\begin{aligned}Y_s=&9.23699\times10^8+2.15357\times10^7\alpha-1.16744\times10^7c+\\&9.76506\times10^6\rho+2.15516\times10^7e+1.19157\times10^7f+\\&3.05592\times10^6v+4.03220\times10^7t_r+4.28517\times10^7w+\\&1.10732\times10^6w^2+1.06528\times10^6\alpha\cdot e+2.00698\times\\&10^6\alpha\cdot v+2.17171\times10^6\rho\cdot w+2.00787\times10^6e\cdot t_r\end{aligned} \tag{41}$$

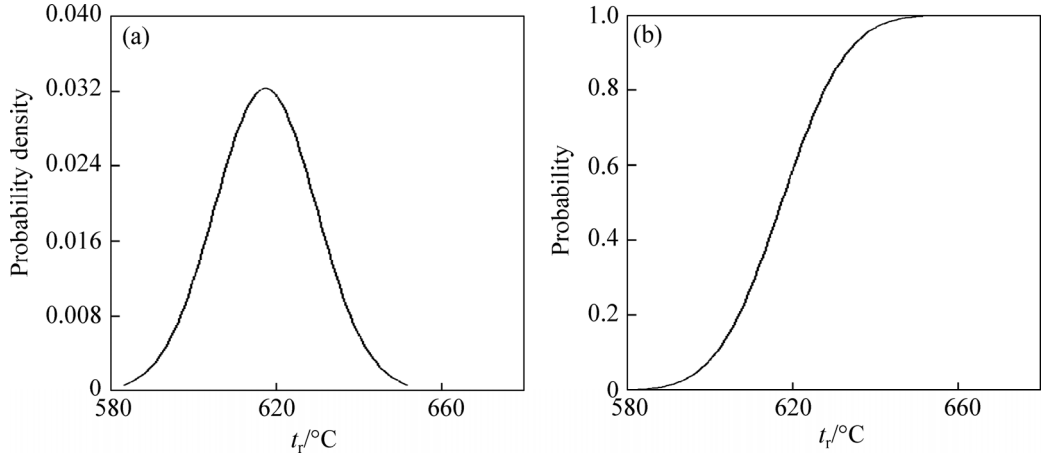

Fig. 8 Probability density (a) and distribution function (b) of temperature

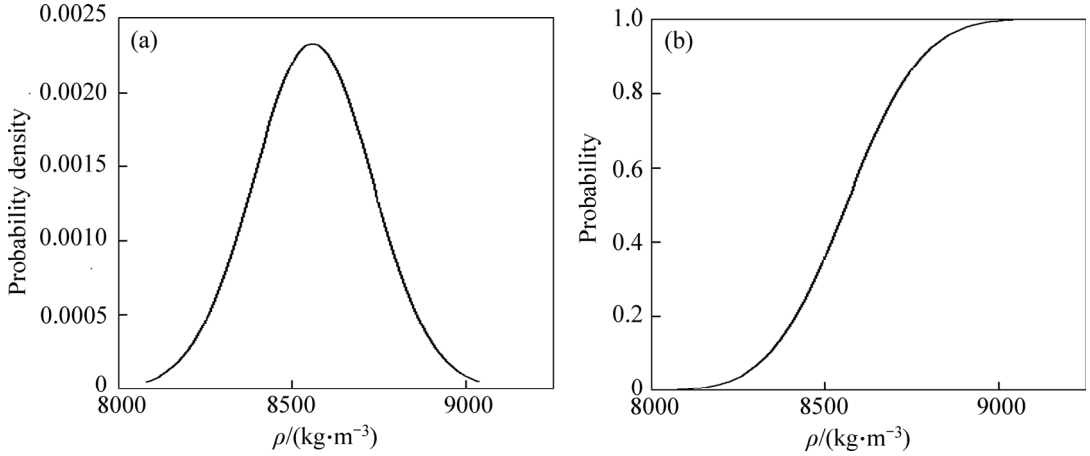

Fig. 9 Probability density (a) and distribution function (b) of material density

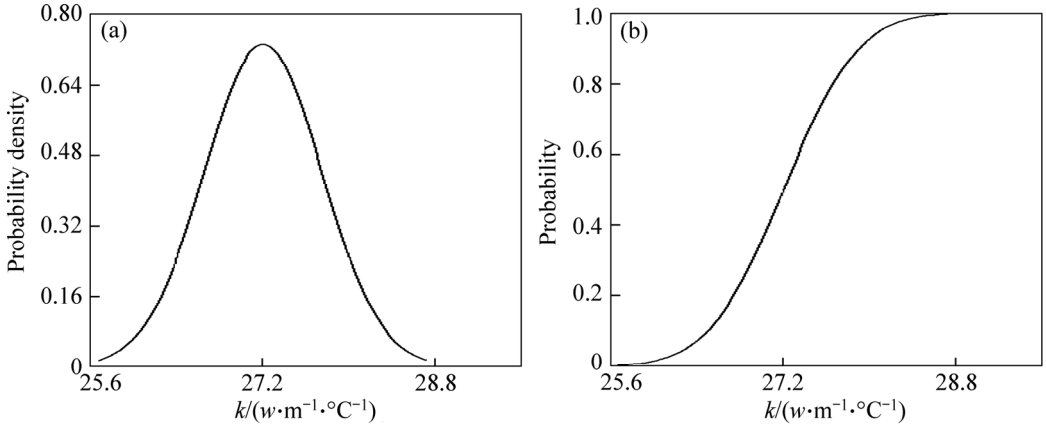

Fig. 10 Probability density (a) and distribution function (b) of heat conductivity coefficient

$$Y_d=1.53729\times10^{-3}-1.08688\times10^{-5}c-1.51030\times10^{-3}e+1.78044\times10^{-5}t_r+3.01880\times10^{-5}w+8.45878\times10^{-6}\alpha+4.22829\times10^{-6}\rho+8.18777\times10^{-6}f+2.67883\times10^{-6}k-2.30861\times10^{-6}v+1.34861\times10^{-6}c^2+1.33499\times10^{-6}\rho^2+2.31917\times10^{-6}e^2+1.71349\times10^{-6}t_r^2+2.31304\times10^{-6}w^2-1.65612\times10^{-7}\alpha\cdot c-1.651101\times10^{-7}c\cdot t_r-2.29585\times10^{-7}\rho\cdot f-3.44358\times10^{-7}\rho\cdot t_r+4.5.778\times10^{-7}\rho\cdot w-4.62045\times10^{-7}e\cdot w+2.65952\times10^{-7}f\cdot t_r \quad (42)$$

FEM of blisk structure is replaced by ERSF and 147 sets of sample points are got using the box-behnken matrix extracting method. Sampling history of stress and total deformation are shown in Fig. 12. Ten thousand samples are extracted by MCS. Simulation samples of stress and total deformation are shown in Fig. 13, cumulative distribution functions are shown in Fig. 14, distribution histograms are shown in Fig. 15, and inverse probabilistic analysis is shown in Table 2.

According to the parameters provided by Table 1, stress distribution and total deformation of bladed disk

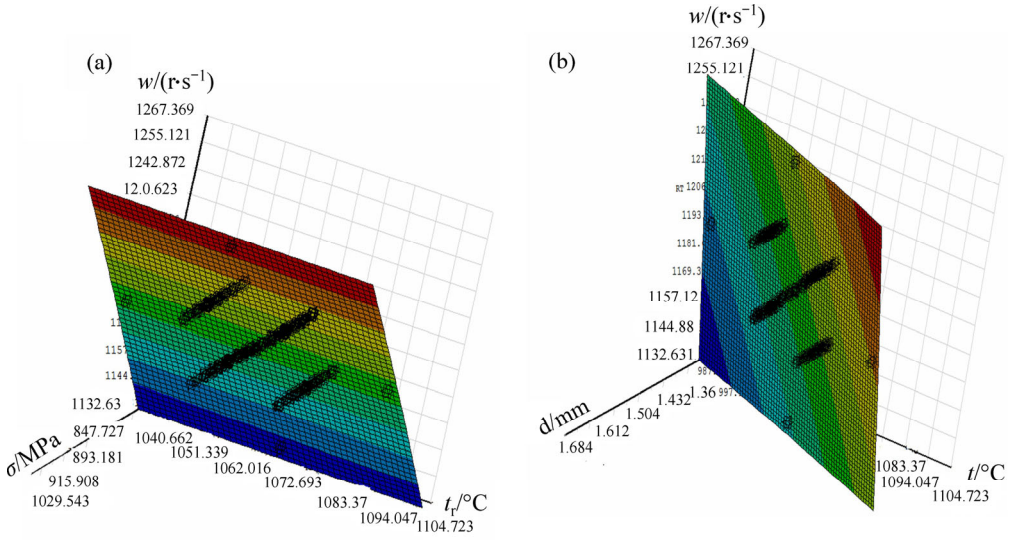

Fig. 11 ERS of stress (a) and total deformation (b)

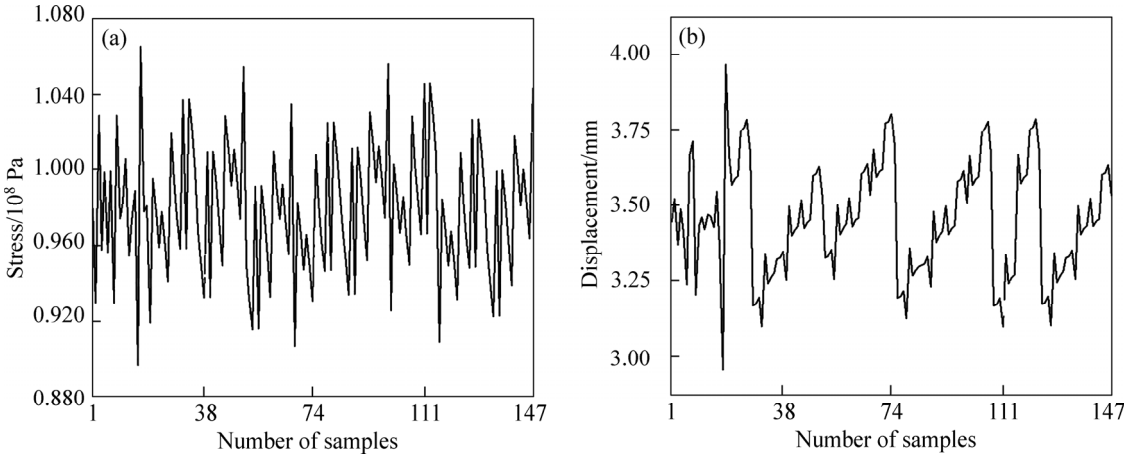

Fig. 12 Sampling history of stress (a) and total deformation (b)

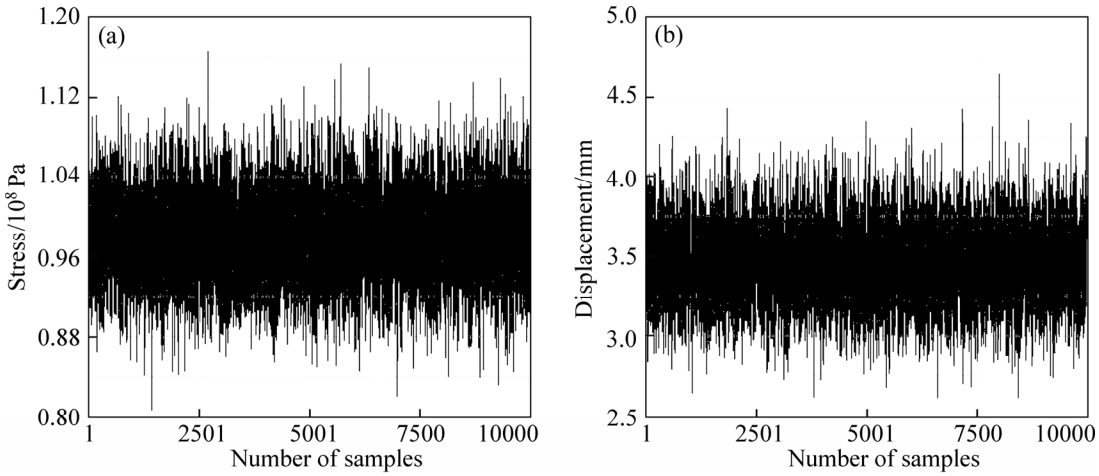

Fig. 13 Simulation samples of stress (a) and total deformation (b)

assemblies are subjected to normal distribution and the mean and standard deviation are 979.24 MPa, 3.452 mm, 4.464 MPa and 0.242 mm, respectively, and the reliability is about 98.99% when the confidence interval is 0.95.

6.3 Sensitivity analysis

Sensitivity is used to analyze the influence degree for the change of the random input variables on the stability of the output parameters and then we can decide which parameters have more heavy impact on the

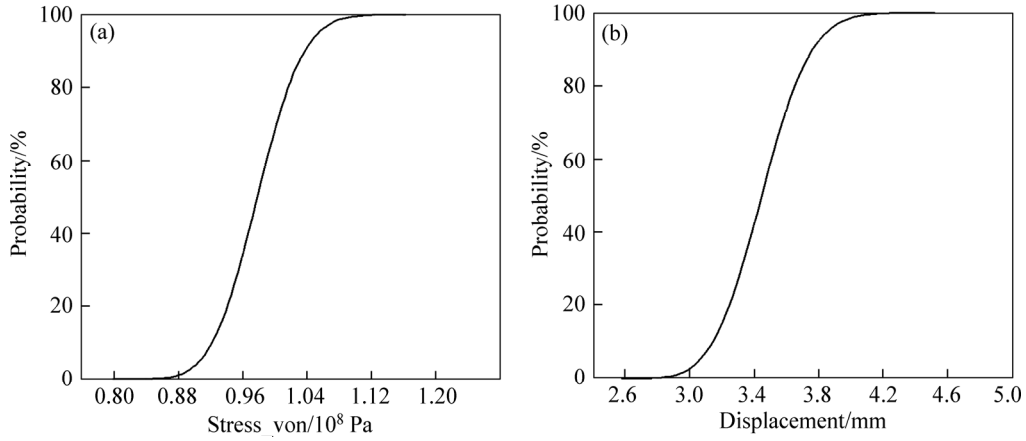

Fig. 14 Cumulative distributions function of stress (a) and total deformation (b)

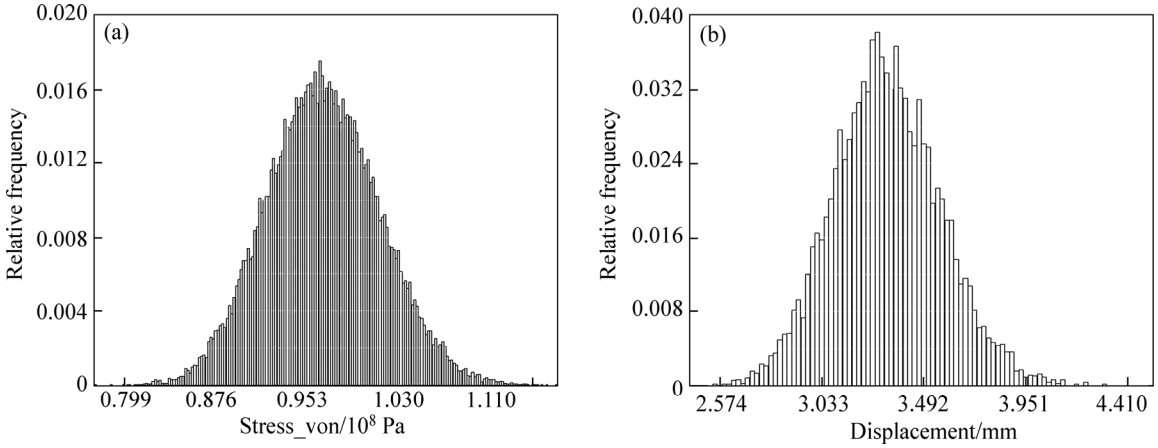

Fig. 15 Distribution histograms of stress (a) and total deformation (b)

Table 2 Limit value of variable under different reliability (parts)

Variable	Reliability, R				
	0.99	0.95	0.90	0.85	0.80
Y_d	3.5231	3.5174	3.4892	3.4769	3.4672
$Y_s/\times10^8$	9.9333	9.7341	9.6247	9.5487	9.4872
w	1094.7	1080.42	1072.81	1067.68	1063.61
$\alpha/10^{-5}$	1.5081	1.4883	1.4779	1.4709	1.4652
k	28.476	28.105	27.908	27.774	27.668
f	3469.2	3423.9	3399.8	3383.6	3370.6
c	523.28	516.45	512.82	510.37	508.42
$e/10^{11}$	1.2454	1.2292	1.2205	1.2147	1.2100
v	0.3289	0.3246	0.3224	0.3208	0.3196
ρ	8958.7	8841.6	8779.4	8737.5	8704.1
t_r	1255.9	1239.5	1230.8	1224.9	1220.2

reliability failure. The sensitivity of every random variable, effect probability and the correlation between stress and total deformation are acquired by Eqs. (22)−(29). The results are shown in Figs. 16 and 17 and Table 3.

The conclusion is gained from Fig. 15 and Table 3 that, the rotational speed and the gas temperature are the main influential factors on stress distribution of bladed disk assemblies, and the effect probabilities are respectively 27.40% and 25.05%. But for the total deformation, the influence of rotational speed is the most obvious and the effect probability is 43.05%, followed by the elastic modulus and density. It is also found that there are positive and negative variables. The positive ones demonstrate that the variable is positively associated with stress and total deformation, while the negative ones demonstrate that the variable might inhibit the increase of stress or deformation. So specific heat capacity increasing may inhibit the increase of stress, while the increase of elastic modulus may inhibit the increase of deformation. Therefore, every factor should be considered and the appropriate measures should be taken to inhibit the increase of them.

6.4 Effectiveness verification

In order to verify the efficiency and accuracy of ERSM which is compared with MCS and RSM based on random input variables and numerical characteristics in Table 1 and the same environmental conditions, DPA of stress distribution and total deformation for bladed disk

Table 3 Sensitivity and effect probability of random input variables of blisk structure

Variable	t_r	α	c	ρ	v	f	k	e	w
$L_1/10^{-3}$	558.77	270.76	−160.84	135.33	36.74	160.84	3.176	292.85	611.19
P_{x1}/%	25.05	12.14	7.21	6.07	1.65	7.21	0.14	13.13	27.40
$L_2/10^{-3}$	−103.45	−92.77	−41.64	355.42	−21.42	18.09	19.03	−408.75	801.69
P_{x2}/%	5.56	4.98	2.24	19.09	1.15	0.97	1.02	21.95	43.05

Note: L_1−Input variables to sensitivity of stress; P_{x1}−Input variables to effect probability of stress; L_2−Input variables to sensitivity of total deformation; P_{x2}−Input variables to effect probability of total deformation.

Table 4 Comparison of three probabilistic analysis methods

Method	t/h	Y_d		Y_s		t_r	
		Mean/mm	Precision/%	Mean/MPa	Precision/%	Effect probability, $(Y_d\|Y_s)$/%	Precision, (Y_dY_s)/%
FE−ERSM	2.25	3.452	99.97	978.24	100	10.89|31.73	93.93|98.45
MCM	153	3.451	100	979.24	100	10.23|31.24	100|100
RSM	6.75	3.437	99.59	981.96	99.72	12.52|30.37	81.71|96.81

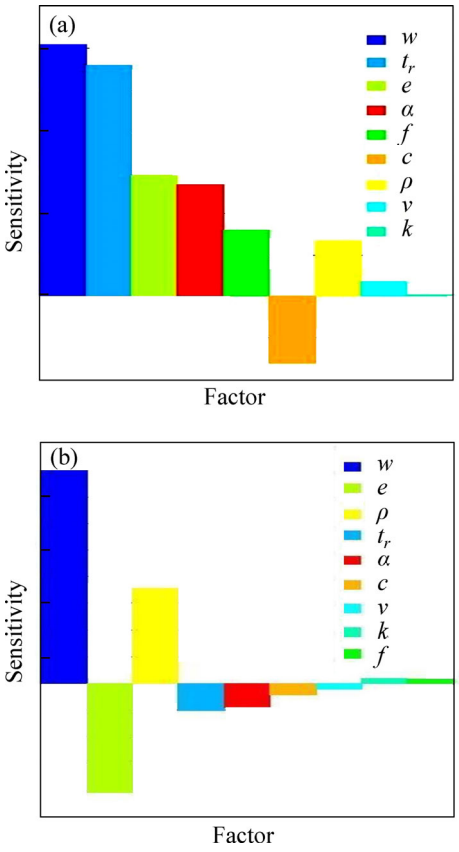

Fig. 16 Sensitivities of stress (a) and total deformation (b)

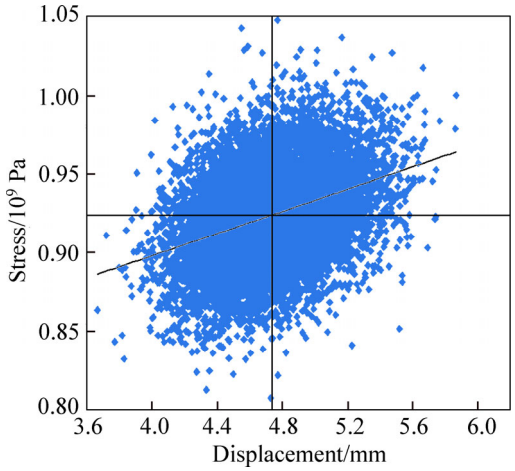

Fig. 17 Correlation between stress and total deformation

assemblies are researched. In the process of calculation, 10000 samples are drawn by the three methods, the numbers are all drawn by ERSM and RSM and the MCS is seem as basic standard. The comparing results are shown in Table 4.

It can be seen from the Table 4, compared with the MCS, the ERSM proposed in this work is higher than the traditional RSM in the computational accuracy and efficiency, and computation time is far less than those of RSM and MCS, nearly equal to 1/68 that of the MC and 1/3 that of RSM, respectively. Obviously, not only computational precision can be ensured but also the computational time is greatly shortened and computational efficiency is improved.

7 Conclusions

1) The ERSM of the DPA is introduced and the mathematical model is established. Meanwhile, the method of reliability calculation and sensitivity analysis are given.

2) The process including start−idling−take off−climbing−cruise of aeroengine is selected as the range, and the coupling impact of temperature load, centrifugal force and coriolis forces are considered. Meanwhile, FEM of blisk is set up, a sector is chosen as the research object and the deterministic analysis of bladed disk assemblies is done. Changing curve with time of output response is obtained, the nodes of the stress distribution and the total deformation are found out and the change rule of them is analyzed.

3) The DPA of stress distribution and total deformation for bladed disk assemblies is investigated by the ERSM. The dynamics and randomness of thermal load, rotational speed, nonlinear factors such as materials are taken into account. And the ERS, the changing patterns of sampling history, simulation sample, cumulative distribution function, and distribution histogram are gotten.

4) Sensitivity analysis of stress distribution and total deformation for bladed disk assemblies is done. Simultaneously, the main influence factors and influence degree of stress concentration and deformation are analyzed.

References

[1] KENYON J A, GRIFFIN J H. Forced response of turbine engine bladed disks and sensitivity to harmonic mistuning [J]. Journal of Engineering for Gas Turbines and Power, 2003, 125(1): 113−120.

[2] KENYON J A, GRIFFIN J H. Experimental demonstration of maximum mistuned bladed disk forced response [J]. Journal of Turbomachinery, 2003, 125(4): 673−681.

[3] KENYON J A, GRIFFIN J H, KIM N E. Sensitivity of tuned bladed disk response to frequency veering [J]. Journal of Engineering for Gas Turbines and Power, 2005, 127(4): 835−842.

[4] KENYON J A, GRIFFIN J H, FEINER D M. Maximum bladed disk forced response from distortion of a structural mode [J]. Journal of Turbomachinery, 2003, 125(2): 352−363.

[5] PETROV E P. A method for forced response analysis of mistuned bladed disks with aerodynamic effects included [J]. Journal of Engineering for Gas Turbines and Power, 2010, 132(6): 062502.1−062502.10.

[6] JUDGE J, PIERRE C, MEHMED O. Experimental investigation of mode localization and forced response amplitude magnification for a mistuned bladed disk [J]. Journal of Engineering for Gas Turbines and Power, 2001, 123: 940−950.

[7] BLADH R, PIERRE C, CASTANIER M P, KRUSE M J. Dynamic response predictions for a mistuned industrial turbomachinery rotor using reduced-order modeling [J]. Journal of Engineering for Gas Turbines and Power, 2002, 124(2): 311−324.

[8] BLADH R, CASTANIER M P, PIERRE C. Reduced order modeling and vibration analysis of mistuned bladed disk assemblies with shrouds [J]. Journal of Engineering for Gas Turbines and Power, 1999, 121(3): 515−522.

[9] CHAN Y J, EWINS D J. Prediction of vibration response levels of mistuned integral bladed disks (blisks): Robustness studies [J]. Journal of Turbomachinery, 2012, 134(4): 044501.1−044501.7.

[10] HSU K, HOYNIAK D. A fast influence coefficient method for aerodynamically mistuned disks aeroelasticity analysis [J]. Journal of Engineering for Gas Turbines and Power, 2011, 133(12): 122502.1−122502.10.

[11] CAPIEZ-LERNOUT E, SOIZE C, LOMBARD J P, DUPONT C, SEINTURIER E. Blade manufacturing tolerances definition for a mistuned industrial bladed disk [J]. Journal of Engineering for Gas Turbines and Power, 2005, 127(3): 621−628.

[12] NIKOLIC M, PETROV E P, EWINS D J. Coriolis forces in forced response analysis of mistuned bladed disks [J]. Journal of Turbomachinery, 2007, 129(4): 730−739.

[13] GURVICH M R, PIPES R B. Probabilistic strength analysis of four-directional laminated composites [J]. Composites Science and Technology, 1996, 56 (6): 649−656.

[14] PUGH C E, BASS B R, DICKSON T L. Role of probabilistic analysis in integrity assessments of reactor pressure vessels exposed to pressurized thermal-shock conditions [J]. Engineering Failure Analysis, 2007, 14(3): 501−517.

[15] LÜ Q, LOW B K. Probabilistic analysis of underground rock excavations using response surface method and SORM [J]. Computers and Geotechnics, 2011, 38(8): 1008−1021.

[16] KARTAL M E, BASAGA H B, BAYRAKTAR A. Probabilistic nonlinear analysis of CFR dams by MCS using response surface method [J]. Applied Mathematical Modelling, 2011, 35(6): 2752−2770.

[17] FITZPATRICK C K, BALDWIN M A, RULLKOETTER P J, PETER J L. Combined probabilistic and principal component analysis approach for multivariate sensitivity evaluation and application to implanted patellofemoral mechanics [J]. Journal of Biomechanics, 2011, 44(1): 13−21.

[18] ALESSANDRO Z, MICHELE B, ANDREA D A, LUIGINO D. Probabilistic analysis for design assessment of continuous steel-concrete composite girders [J]. Journal of Constructional Steel Research, 2010, 66(7): 897−905.

[19] NAKAMURA T, FUJII K. Probabilistic transient thermal analysis of an atmospheric reentry vehicle structure [J]. Aerospace Science and Technology, 2006, 10(4): 346−354.

[20] TAN Xiao-hui, BI Wei-hua, HOU Xiao-liang,WANG Wei. Reliability analysis using radial basis function networks and support vector machines [J]. Computers and Geotechnics, 2011, 38(2): 178−186.

[21] MOLLON G, DIAS D, SOUBRA A H. Probabilistic analysis of pressurized tunnels against face stability using collocation based stochastic response surface method [J]. Journal of Geotechnical & Geoenvironmental Engineering, 2011, 137(4): 385−397.

[22] REN Yuan, BAI Guang-chen, HAN S Y. New neural network response surface methods for reliability analysis [J]. Chinese Journal of Aeronautics, 2011, 24(1): 65−72.

[23] EOM Y S, YOO K S, PARK J Y, HAN S Y. Reliability-based topology optimization using a standard response surface method for three-dimensional structures [J]. Structural and Mltidisciplinary Optimization, 2011, 43(2): 287−295.

[24] MELCHERS R E, AHAMMED M. A fast approximate method for parameter sensitivity estimation in Monte-Carlo reliability [J]. Computers and Structures, 2004, 82(1): 55−61.

[25] AHAMMED M, MELCHERS R E. Gradient and parameter sensitivity estimation for systems evaluated using Monte-Carlo analysis [J]. Reliability Engineering and System Safety, 2006, 91(5): 594−601.

[26] KARTAL M E, BASAGA H B, BAYRAKTAR A. Probabilistic nonlinear analysis of CFR dams by MCS using response surface method [J]. Applied Mathematical Modelling, 2011, 35(6): 2752−2770.

[27] LI Chao-yang , ZHANG Yan-chun. Calculation and analysis of the transient 3-Dimensional temperature and stress field of a gas turbine's disk [J]. Journal of Power Engineering, 2006, 26(2): 211−214. (in Chinese)

[28] GUAN Lei, WANG Jia-dao, CHEN Da-rong. 3-D finite element analysis of microengine cylinder temperature field and heat deformation [J]. Journal of Tsinghua University (Sci & Tech), 2003, 43(11): 1487−1490. (in Chinese).

[29] FORSSELL L S. Flight clearance analysis using global nonlinear optimisation-based search algorithms [C]// Proceedings of the AIAA Guidance, Navigation, and Control Conference. New York: AIAA, 2003: 1−8.

[30] KYPUROS J A, MELCHER K J. A reduced model for prediction of thermal and rotational effects on turbine tip clearance [R]. Washington DC: NASA, 2003.

(Edited by FANG Jing-hua)